Volume 15 Issue 4 April 2007 ISSN 0967-0661

ELSEVIER

CONTROL ENGINEERING PRACTICE

A Journal of IFAC the International Federation of Automatic Control

CONTENTS

Continued on back cover

Available online at
ScienceDirect
www.sciencedirect.com

IFAC

Available online at www.sciencedirect.com
ScienceDirect
Control Engineering Practice 15 (2007) 447–457
CONTROL ENGINEERING PRACTICE
www.elsevier.com/locate/conengprac

Backlash phenomenon observation and identification in electromechanical system

R. Merzouki[a,*], J.A. Davila[b], L. Fridman[b], J.C. Cadiou[c]

[a]LAGIS UMR CNRS 8146, Ecole polytechnique de Lille, Avenue Paul Langevin, 59655 Villeneuve d'Ascq, France
[b]Department of Postgraduate Study, Engineering Faculty, National Autonomous University of Mexico, Mexico D.F.
[c]Laboratoire de Robotique de Versailles, 10-12 avenue de l'Europe, 78140 Vélizy, France

Received 19 June 2005; accepted 6 September 2006
Available online 18 October 2006

Abstract

In this paper a second order sliding mode observer with finite time convergence is developed for an electromechanical system with backlash. As a consequence of finite time convergence the sliding mode equivalent control is used to apply identification algorithms in order to characterize the backlash phenomenon. The dead zone amplitude and the disturbing torque are identified asymptotically. Simulation and experimental tests applied to an electromechanical actuator are given to support the theoretical development.

Keywords: Sliding mode; Disturbing torque; Electromechanical actuator; Dead zone; Adaptive identification

1. Introduction

The observation of mechanical systems is a difficult task due to nonlinearity and discontinuity of their dynamics. In such a case, the usage of sliding mode observers (see for example Utkin, Guldner, & Shi, 1999) seems to be a reasonable choice due to the main advantages of sliding modes: robustness with respect to uncertainties and finite time convergence (Almeida & Alvarez, 2004; Orlov, Alvarez, & Acho, 2000; Shtessel, Shkolnikov, & Brown, 2003).

A new generation of differentiators (Levant, 1998) and observers, based on the second order sliding mode algorithms, have been recently developed. In Shtessel et al. (2003), an asymptotic convergence of error was developed, based on second order siding mode. A sliding mode observer designed via an extension of the invariance principle was applied for systems with Coulomb friction in Orlov et al. (2000).

The application of sliding modes in system observation allows to use algorithms, either via the control equivalent value for perturbation identification and/or linear regression to identify the system parameters (Davila & Fridman, 2004; Utkin et al., 1999).

In mechanical systems, the *backlash* phenomenon becomes a mechanical imperfection when the dead zone amplitude affects the system performance during its control in a closed loop. Some work has already been carried out on comparable systems. This work can be arranged into three main categories: those where the main interest was the control and fault detection and isolation of similar systems, for example adaptive control in Tao and Kokotovic (1995), variable structure control in Tenreiro Machado (1996), trajectory planning and feedforward design for electromechanical motion systems in Lambrechts, Boerlage, and Steinbuch (2005), observer model-based in Dixon (2004) and adaptive estimation and compensation in Merzouki, Cadiou, and M'Sirdi (2004). Those specialized rather in the dynamic analysis of the system (for example in Allan & Levy, 1980; Barbosa & Tenreiro Machado, 2002; Shaw & Rand, 1989) and those where the development is mainly dedicated to the simulation of such systems (see for example in Thompson & Ghaffari, 1982).

*Corresponding author. Tel.: +33 328 767486; fax: +33 328 767301.
E-mail addresses: Rochdi.Merzouki@polytech-lille.fr (R. Merzouki), jadavila@servidor.unam.mx (J.A. Davila), lfridman@servidor.unam.mx (L. Fridman), cadiou@lrv.uvsq.fr (J.C. Cadiou).

0967-0661/$ - see front matter © 2006 Published by Elsevier Ltd.
doi:10.1016/j.conengprac.2006.09.001

List of notation

j_0	dead zone amplitude (rad)
w	nonlinear transmitted torque (N m)
$\tilde{w}$	nonlinear transmitted torque error (N m)
J_e	motor inertia (N m^2)
J_s	load inertia (N m^2)
K	elasticity constant (N m/rad)
N_0	reducer constant
f_e	viscous friction coefficient in the motor side (N m s/rad)
f_s	viscous friction coefficient in the load side (N m s/rad)
θ_e	input reducer position (rad)
$\dot{\theta}_e$	input reducer velocity (rad/s)
$\ddot{\theta}_e$	input reducer acceleration (rad/sec^2)
θ_s	output reducer position (rad)
$\dot{\theta}_s$	output reducer velocity (rad/s)
$\ddot{\theta}_s$	output reducer acceleration (rad/s^2)

In some cases, for a better understanding of the backlash mechanism, the reconstruction of nonmeasurable states is needed. For this purpose, the used observers require to keep the finite time convergence even if the system exhibits the backlash phenomenon.

In this paper, two nonlinear observers, based on the second order sliding mode super-twisting algorithm Levant (1993) are developed. They reconstruct input and output velocities for mechanical system with backlash phenomenon, using position measurements. The finite time convergence of these observers allows to use properties of equivalent control to identify the backlash as a perturbation, or in a no disturbing frame, using linear regression algorithms to identify the backlash parameters.

An important implementation restriction of linear regression algorithm is the persistent excitation condition required for the signal to be sufficiently rich ensuring the matrix inversion, and which include all the known functions of the system. In this paper, the matrix dimensions in the persisting condition are reduced by using only unknown parameters in the regressor structure.

The remainder of this paper is organized as follows. The next section describes the electromechanical test bench. Section 3 describes the backlash modeling and Section 4 presents the developed super-twisting observer to estimate the disturbing backlash torque and the dead zone amplitude. Sections 5 and 6 present simulation and experimental results, respectively. Conclusion is given in Section 7 and at last, the algorithm convergence proof is given in the Appendix.

2. Electromechanical actuator description and modeling

The test bench presented in Fig. 1 has been developed to identify some mechanical imperfections. All of this development is given in Merzouki and Cadiou (2005). It represents an electromechanical system made up of a motor reducer involving an external load. The motor part is actuated by a DC motor delivering a relative important mass torque. This test bench presents built-in mechanical imperfections as friction, backlash and elasticity and allows to vary their amplitudes. Coulomb friction is represented by a contact of various components of the system with different rigidities. Viscous friction depends on the lubricant viscosity, contained between surfaces in contact. Backlash phenomenon is described by two independent mechanical parts, whose transmission is carried out via a dead zone, varying between 0° and 24°. A spring system is placed between the two mechanical parts in order to deliver a smooth transmission.

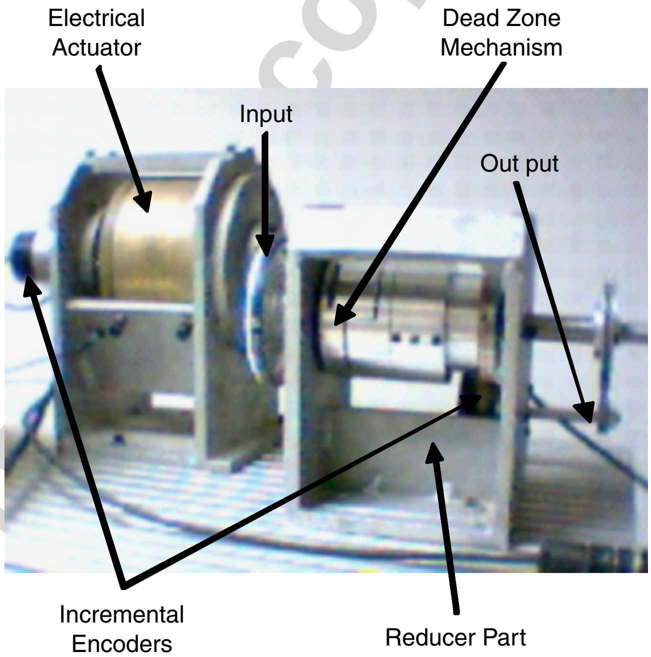

Fig. 1. Electromechanical test bench.

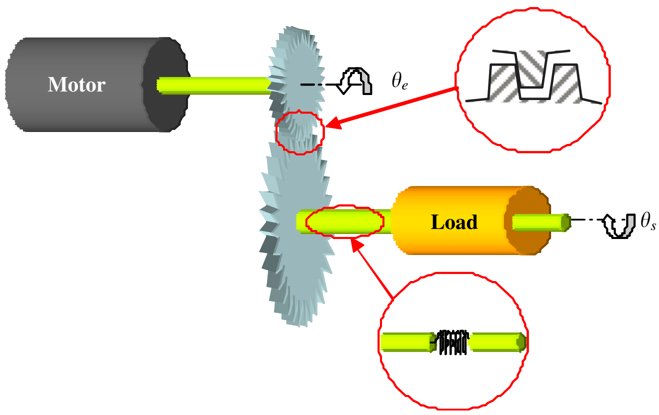

Fig. 2. Electromechanical system including mechanical imperfections.

On this test bench, one can measure input and output positions of the reducer part by using two incremental encoders of Fig. 1, where the relative load position is depending on friction between the gears in contact, as well as flexible transmission through a dead zone. Fig. 2 illustrates the simplified system schema of the real system.

Let us consider that static friction is disregarded, then the mechanical model of the test bench, including the backlash is described by the following system

$$\begin{cases} J_e.\ddot{\theta}_e + f_e.\dot{\theta}_e + C = u, \\ J_s.\ddot{\theta}_s + f_s.\dot{\theta}_s = N_0.C, \end{cases} \tag{1}$$

J_s, J_e, f_s, f_e are, respectively, inertias and viscous frictions of reducer and motor parts which are identified experimentally.

$\ddot{\theta}_s$, $\ddot{\theta}_e$, $\dot{\theta}_s$, $\dot{\theta}_e$ are, respectively, accelerations and velocities of reducer and motor parts which are deduced by derivation of the measured input and output positions θ_s and θ_e.

u, C, N_0 are, respectively, control input torque, transmitted torque via the dead zone and reduction constant.

Introducing the variables $x_{1e} = \theta_e$, $x_{1s} = \theta_s$, $x_{2e} = \dot{\theta}_e$, $x_{2s} = \dot{\theta}_s$, model (1) can be rewritten as

$$\begin{cases} \dot{x}_{1e} = x_{2e}, \\ \dot{x}_{1s} = x_{2s}, \\ \dot{x}_{2e} = -\dfrac{f_e}{J_e}.x_{2e} + \dfrac{u}{J_e} - \dfrac{C}{J_e}, \\ \dot{x}_{2s} = -\dfrac{f_s}{J_s}.x_{2s} + \dfrac{N_0.C}{J_s}. \end{cases} \tag{2}$$

3. Backlash torque modeling

Generally, modeling of the mechanical torque, transmitted through a dead zone and a flexible axis (see in Fig. 2), is given by a nonlinear and noncontinuous function of Fig. 3(b). Unfortunately, the noncontinuous characteristic of the transmitted torque around the contact areas, can make the system observation and control difficult. Thus, and in order to avoid this noncontinuous property, once thought of bringing a flexible bond inside the dead zone areas of the electromechanical system (see Fig. 3(a)). It describes a *body*1 trying to transmit motion to *body*2 via a dead zone of amplitude $2j_0$. The transmission will be correct when the two bodies are in contact (i.e. the two positions are identical). Otherwise (the bodies are not in contact), the transmission will be delayed due to the presence of a dead zone. This physical modification allows avoiding some undesirable behavior following the shocks between the various parts of the system and at the same time to simplify the noncontinuous model and make it rich in information about modulated dead zone and flexibility of the transmission link. All the mechanical characteristics and modeling about the test bench system are developed in Merzouki and Cadiou (2005).

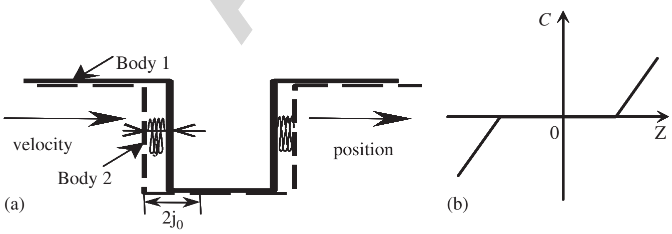

Fig. 3. (a) Backlash mechanism; (b) noncontinuous backlash model.

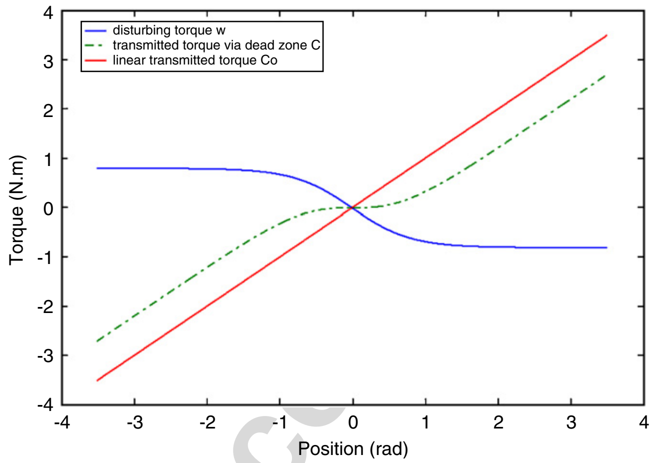

Fig. 4. Approximation of transmitted torques.

So, a smooth and continuous model (see Fig. 4) of transmitted torque C, expressed in (3), is chosen to be identified in the next sections as perturbation or unknown linear parameters function. This latter includes a sigmoid function expressed as follows:

$$C = K.\left(z - 4.j_0.\frac{1 - e^{-\gamma.z}}{1 + e^{-\gamma.z}}\right), \tag{3}$$

where C is the approximate transmitted torque, $z = x_{1e} - N_0.x_{1s}$ defines the difference between input and output reducer positions, K the rigidity parameter, j_0 the dead zone amplitude and γ the slope constant.

One can decompose (3) into two parts

$$C = C_0 + w \tag{4}$$

with C_0 the linear transmitted torque describing a flexible link and is given by the linear formulation

$$C_0 = K.z \tag{5}$$

and w is the disturbing and nonlinear transmitted torque expressed by

$$w = -4.K.j_0.\frac{1 - e^{-\gamma.z}}{1 + e^{-\gamma.z}}. \tag{6}$$

Since the real backlash amplitude j_0 is equal to a constant, its variation is null.

The disturbing torque w have a sigmoid function form, characterized by its decreasing slope constant γ, identified in Merzouki et al. (2004) and chosen to give the best approximation of the transmitted torque inside the dead zone $[-j_0, +j_0]$.

4. Observer design

The proposed observer has the form

$$\begin{cases} \dot{\hat{x}}_{1e} = \hat{x}_{2e} + z_{1e}, \\ \dot{\hat{x}}_{1s} = \hat{x}_{2s} + z_{1s}, \\ \dot{\hat{x}}_{2e} = -\dfrac{f_e}{J_e}.\hat{x}_{2e} + \dfrac{u}{J_e} + z_{2e}, \\ \dot{\hat{x}}_{2s} = -\dfrac{f_s}{J_s}.\hat{x}_{2s} + z_{2s}, \end{cases} \tag{7}$$

where $\hat{x}_{1e}$, $\hat{x}_{1s}$, $\hat{x}_{2e}$ and $\hat{x}_{2s}$ are the state estimations, z_{1e}, z_{1s}, z_{2e} and z_{2s} are the correction factors based on the super-twisting algorithm (see Fig. 5) and are given by the formulas

$$\begin{cases} z_{1e} = \lambda_1 |x_{1e} - \hat{x}_{1e}|^{1/2} \operatorname{sign}(x_{1e} - \hat{x}_{1e}), \\ z_{2e} = \alpha_1 \operatorname{sign}(x_{1e} - \hat{x}_{1e}), \\ z_{1s} = \lambda_2 |x_{1s} - \hat{x}_{1s}|^{1/2} \operatorname{sign}(x_{1s} - \hat{x}_{1s}), \\ z_{2s} = \alpha_2 \operatorname{sign}(x_{1s} - \hat{x}_{1s}) \end{cases} \tag{8}$$

and the parameters α_i and λ_i are designed so as to fulfill the conditions

$$\alpha_i > f_i^+,$$
$$\lambda_i > \sqrt{\frac{2}{\alpha - f_i^+}} \frac{(\alpha_i + f_i^+)(1 + q_i)}{(1 - q_i)},$$

where $i = 1, 2$, the constants $f_1^+ = 2 \max \ddot{x}_{2e}, f_2^+ = 2 \max \ddot{x}_{2s}$, and $0 < q_i < 1$ (Davila & Fridman, 2004).

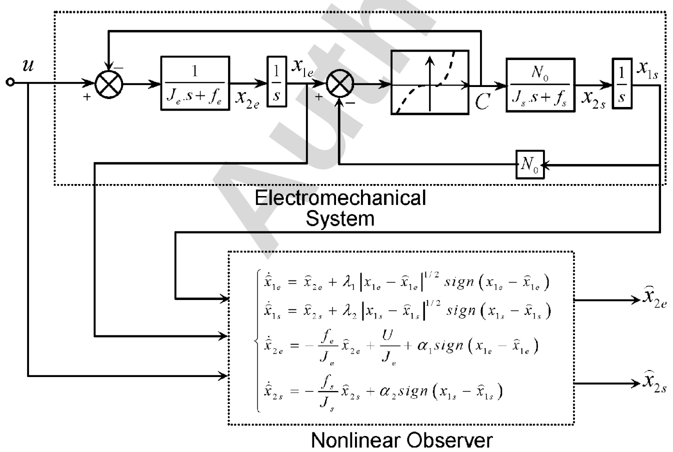

Fig. 5. Super-twisting observer structure.

Then the state observation error is expressed as

$$\begin{cases} \dot{\tilde{x}}_{1e} = \tilde{x}_{2e} - \lambda_1 |\tilde{x}_{1e}|^{1/2} \operatorname{sign}(\tilde{x}_{1e}), \\ \dot{\tilde{x}}_{1s} = \tilde{x}_{2s} - \lambda_2 |\tilde{x}_{1s}|^{1/2} \operatorname{sign}(\tilde{x}_{1s}) \\ \dot{\tilde{x}}_{2e} = -\dfrac{f_e}{J_e}.\tilde{x}_{2e} - \dfrac{C}{J_e} - \alpha_1 \operatorname{sign}(\tilde{x}_{1e}), \\ \dot{\tilde{x}}_{2s} = -\dfrac{f_s}{J_s}.\tilde{x}_{2s} + \dfrac{CN_0}{J_s} - \alpha_2 \operatorname{sign}(\tilde{x}_{1s}). \end{cases} \tag{9}$$

Using these observers ensure the finite time convergence of observation states error to zero. In this case, a finite time convergence of the estimated states to the real states values is obtained. Convergence proof is given in the Appendix.

4.1. Perturbation identification

As a consequence of finite time convergence and the existence of a equivalent control ensuring the sliding motion is guaranteed (Utkin et al., 1999). This equivalent control ensuring the sliding motion, allows to directly identify the external perturbations acting on the system.

In order to perform perturbation identification, each couple of the system coordinates (x_{1e}, x_{2e}) and (x_{1s}, x_{2s}) (2) has the following representation:

$$\begin{cases} \dot{x}_1 = x_2, \\ \dot{x}_2 = f(t, x_1, x_2, u) + \xi. \end{cases} \tag{10}$$

System (10) can be rewritten in a more general form as

$$\begin{cases} \dot{x}_1 = x_2, \\ \dot{x}_2 = a\varphi(t, x_1, x_2, u) + \xi, \end{cases} \tag{11}$$

where a is a vector of parameters, $\varphi(t, x_1, x_2, u)$ is a vector of all the state functions in the electromechanical system and ξ is a perturbation term.

In the case where the nonlinear transmitted torque is unknown, it would be practical to consider it as a perturbation. Then, the following perturbation definition is deduced from (9):

$$\xi = \begin{cases} -\dfrac{C}{J_e}: & \text{for motor part,} \\ \dfrac{N_0 C}{J_s}: & \text{for reducer part.} \end{cases}$$

Then, the super-twisting observer is given by

$$\begin{cases} \dot{\hat{x}}_1 = \hat{x}_2 + \lambda |\tilde{x}_1|^{1/2} \operatorname{sign}(\tilde{x}_1), \\ \dot{\hat{x}}_2 = \bar{a}\varphi(t, x_1, \hat{x}_2, u) + \alpha \operatorname{sign}(\tilde{x}_1), \end{cases} \tag{12}$$

where $\bar{a}$ is a vector of nominal values of the parameter vector a. The equations for the error become

$$\begin{cases} \dot{\tilde{x}}_1 = \tilde{x}_2, \\ \dot{\tilde{x}}_2 = \Delta a\, \varphi(t, x_1, \tilde{x}_2, u) + \xi - \alpha \operatorname{sign}(\tilde{x}_1). \end{cases} \tag{13}$$

The finite time convergence of x_1 and x_2 allows to write

$$z_2 = \alpha \operatorname{sign}(\tilde{x}_1) = \Delta a\, \varphi(t, x_1, \tilde{x}_2, u) + \xi, \tag{14}$$

with $\Delta a = a - \bar{a}$ and $\varphi(t, x_1, \tilde{x}_2, u)$ is a nonlinear vector containing all the states functions.

It is assumed that the term z_2 changes at a high, theoretically infinite frequency. However, in practice, various imperfections make the state oscillate in some vicinity of the intersection, whereas the components of z_2 are switched at finite high frequency. The high frequency term z_2 is filtered out and the motion in the sliding mode is determined by the slow component (Utkin et al., 1999). It is reasonable to assume that the equivalent control is close to the slow component of the real control. The latter may be derived by filtering out the high frequency component using a lowpass filter. The filter time constant should be sufficiently small to preserve the slow component but large enough to eliminate the high frequency component.

After using $\bar{z}_2$, the filtered version of z_2, expression (14) can be formulated as

$$\bar{z}_2 = \alpha \operatorname{sign}(\tilde{x}_1) = \Delta a\, \varphi(t, x_1, \tilde{x}_2, u) + \xi. \tag{15}$$

When the parameters of the system are totally known, i.e.

$$a = \bar{a} = \begin{cases} -\dfrac{f_e}{J_e}: \text{ for motor part,} \\ -\dfrac{f_s}{J_s}: \text{ for reducer part,} \end{cases} \tag{16}$$

the term $\Delta a = 0$ (see Fig. 6) and $\bar{z}_2$ gives an estimation of the perturbation ξ

$$\bar{z}_2 = \alpha \operatorname{sign}(\tilde{x}_1) = \xi. \tag{17}$$

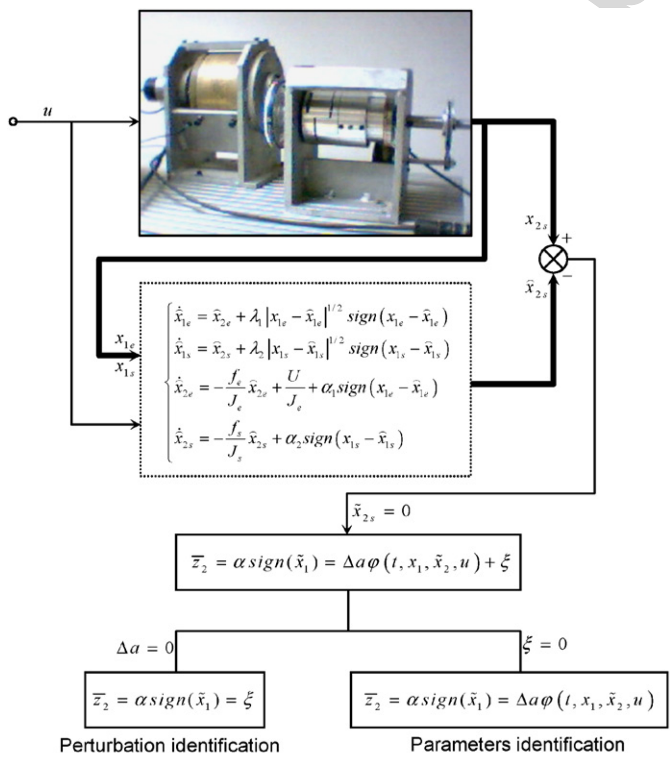

Fig. 6. Perturbation and parameter identification schema.

4.2. Parameter identification

In the case when the transmitted torque C is modelled as described in Section 3, in the absence of any perturbation (i.e. $\xi = 0$), let us consider that only nominal values of the system parameters are known (see Fig. 6). Then, the use of equivalent control, in combination with identification algorithms, allows to identify the real values of system parameters.

After a finite time duration, the next equality holds for $\bar{z}_2$:

$$\bar{z}_2 = \alpha \operatorname{sign}(\tilde{x}_1) = \Delta a\, \varphi(t, x_1, \tilde{x}_2, u), \tag{18}$$

where $\Delta a = a - \bar{a}$, equality (18) has the model structure for linear regression (Soderstrom & Stoica, 1989)

$$h(t) = \Theta \varphi(t), \tag{19}$$

where $h(t)$ is a measurable quantity, Θ is a vector of unknown parameters to be identified, $\varphi(t)$ is a vector of known quantities. Defined in our case $\Theta = \Delta a$, $h(t) = \bar{z}_2$ and

$$\varphi(t) = \begin{cases} \begin{pmatrix} -\dfrac{z}{J_e} \\ \dfrac{4}{J_e}\dfrac{1 - e^{-\gamma.z}}{1 + e^{-\gamma.z}} \end{pmatrix} & \text{for motor part,} \\ \begin{pmatrix} \dfrac{N_0 z}{J_s} \\ -\dfrac{4N_0}{J_e}\dfrac{1 - e^{-\gamma.z}}{1 + e^{-\gamma.z}} \end{pmatrix} & \text{for reducer part,} \end{cases} \tag{20}$$

where $z = \theta_e - N_0\ \theta_s$, is the measured difference position between motor and reducer parts, N_0 the reduction constant, γ is a decreasing slope constant, supposedly known in the nonlinear sigmoid function and J_e, J_s are, respectively, the electromechanical inertias. The uncertain part is defined as

$$\Delta a^{\mathrm{T}} = (K \quad Kj_0), \tag{21}$$

where K is the transmission constant stiffness and j_0 is the dead zone amplitude. One may notice in (20), the known part of the system used in (7) is not taken into account, as it is not an uncertain part. Then, its value in (18) is equal to zero, leading to reduce the order of the matrix $\varphi(t)$ and, as a consequence, making the fulfillment of the persistent excitation condition easier (Soderstrom & Stoica, 1989).

In this case, Δa is considered a constant vector, taking the value of $h(t) = \bar{z}_2$. It is possible to apply a linear regression algorithm like the least square method to identify dynamic system parameters. Developing least square algorithm, the average expression of time integration with σ as auxiliary time variable is given by

$$\frac{1}{t}\int_0^t \bar{z}_2(\sigma)\varphi(\sigma)^{\mathrm{T}}\,\mathrm{d}\sigma = \Delta a\, \frac{1}{t}\int_0^t \varphi(\sigma)\varphi(\sigma)^{\mathrm{T}}\,\mathrm{d}\sigma, \tag{22}$$

therefore, the parameters can be estimated as

$$\widehat{\Delta a} = \left[\int_0^t \bar{z}_2(\sigma)\varphi(\sigma)^{\mathrm{T}}\,\mathrm{d}\sigma\right]\left[\int_0^t \varphi(\sigma)\varphi(\sigma)^{\mathrm{T}}\,\mathrm{d}\sigma\right]^{-1}, \tag{23}$$

where $\widehat{\Delta a}$ is the estimation of Δa.

Defining $\Gamma_t = [\int_0^t \varphi(\sigma)\varphi(\sigma)^{\mathrm{T}}\,\mathrm{d}\sigma]^{-1}$ along with the equalities

$$\Gamma_t^{-1}\Gamma_t = I,$$

$$\Gamma_t^{-1}\dot{\Gamma}_t + \dot{\Gamma}_t^{-1}\Gamma_t = 0, \tag{24}$$

a parameter estimation algorithm can be written. From (23), the following equation is obtained:

$$\dot{\widehat{\Delta a}} = \left[\int_0^t \bar{z}_2(\sigma)\varphi(\sigma)^{\mathrm{T}}\,\mathrm{d}\sigma\right]\dot{\Gamma}_t + \bar{z}_2\varphi^{\mathrm{T}}\Gamma_t, \tag{25}$$

using Eq. (24), then Eq. (25) is written as follows:

$$\dot{\widehat{\Delta a}} = \widehat{\Delta a}\Gamma_t^{-1}\dot{\Gamma}_t + \bar{z}_2\varphi^{\mathrm{T}}\Gamma_t, \tag{26}$$

using the equalities of Γ_t given above, the dynamic expression to compute $\widehat{\Delta a}$ is given by

$$\dot{\widehat{\Delta a}} = [-\widehat{\Delta a}\,\varphi + \bar{z}_2]\varphi^{\mathrm{T}}\Gamma_t. \tag{27}$$

A dynamic form to find Γ_t is

$$\dot{\Gamma}_t = -\Gamma_t\varphi\varphi^{\mathrm{T}}\Gamma_t. \tag{28}$$

The use of Eqs. (27) and (28) ensures the asymptotic convergence of $\widehat{\Delta a}$ to Δa. These equations allow to identify the real values of the parameters K and j_0.

5. Simulation results

For the simulation tests, a variable velocity trajectory tracking is carried out in the system model set up of Fig. 1. After the injection of a sinusoidal control signal, see Fig. 7, the corresponding simulation constants are given in Table 1. The value of γ represents a nominal value taken from the experimental test bench. For input velocity estimation of Fig. 8, one can notice a good performance of the estimation with an asymptotic convergence of the error in Fig. 9. Then, the input position estimation deduction of Fig. 10 shows that the position estimation error goes also to zero (see Fig. 11). Similarly, the state

Table 1
Simulation model parameters

Observers parameters		System parameters	
α_1	1.8	J_s	7
α_2	0.08	f_s	16
λ_1	0.005	N_0	5
λ_2	0.004	J_m	0.05
		f_m	0.15
		γ	20
		K	1

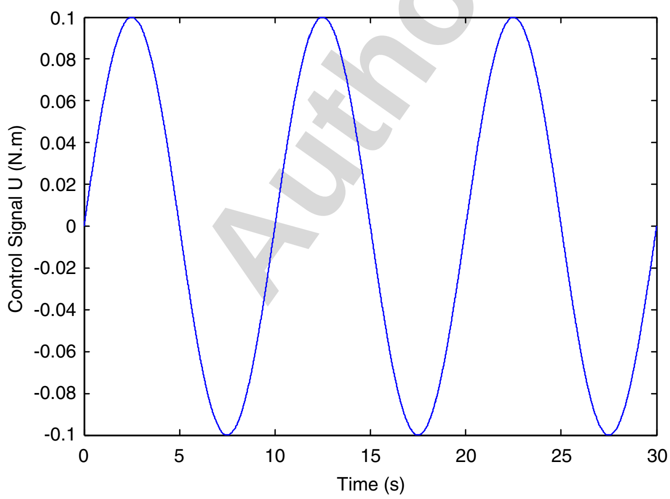

Fig. 7. Applied control signal.

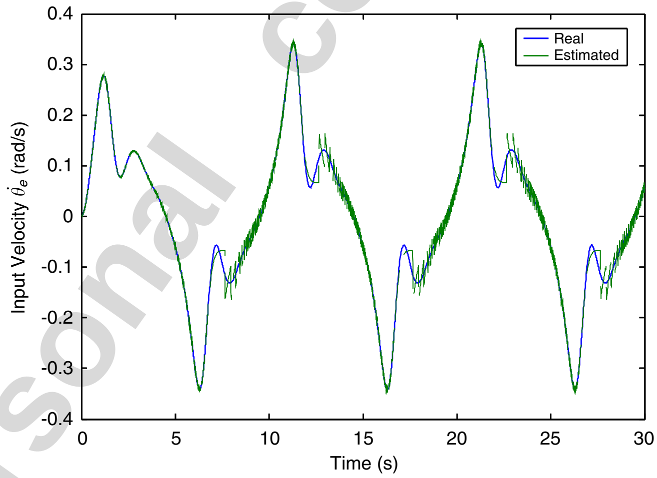

Fig. 8. Estimation of input velocity signal.

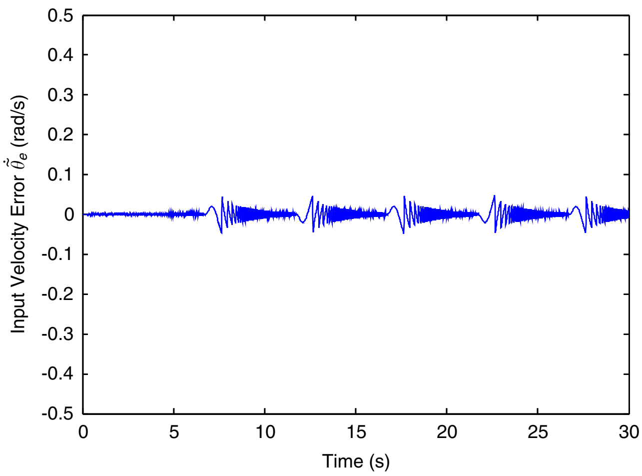

Fig. 9. Input velocity estimation error.

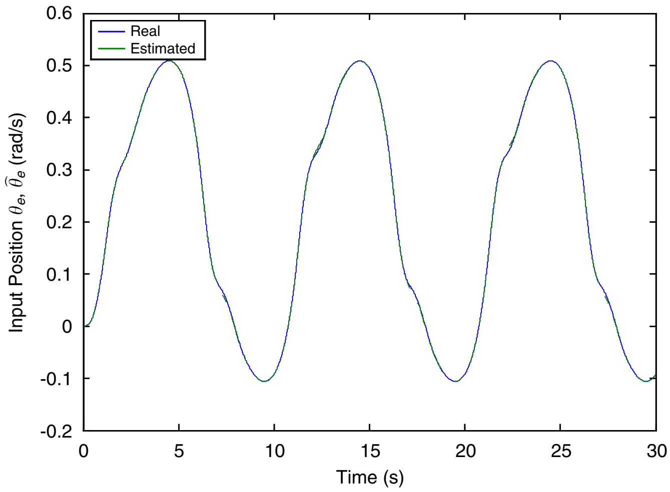

Fig. 10. Estimation of input position signal.

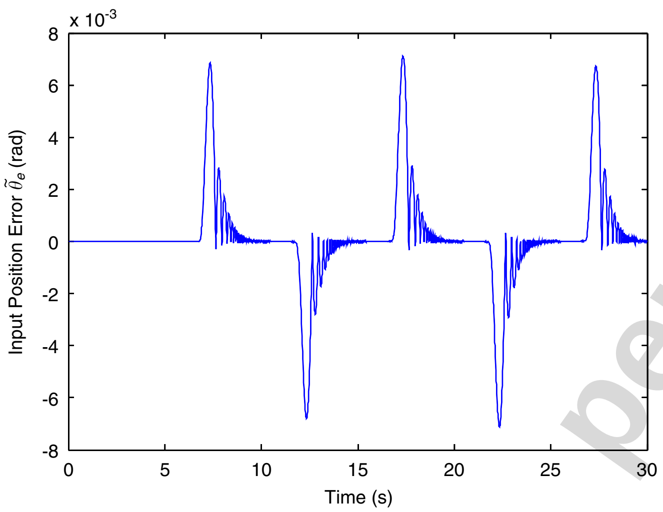

Fig. 11. Input position estimation error.

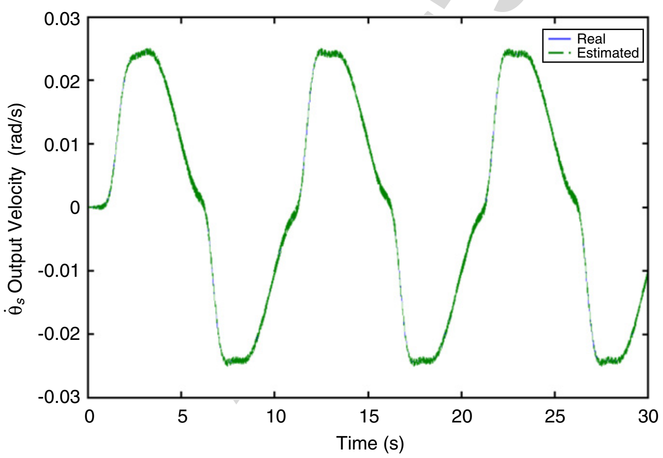

Fig. 12. Estimation of output velocity signal.

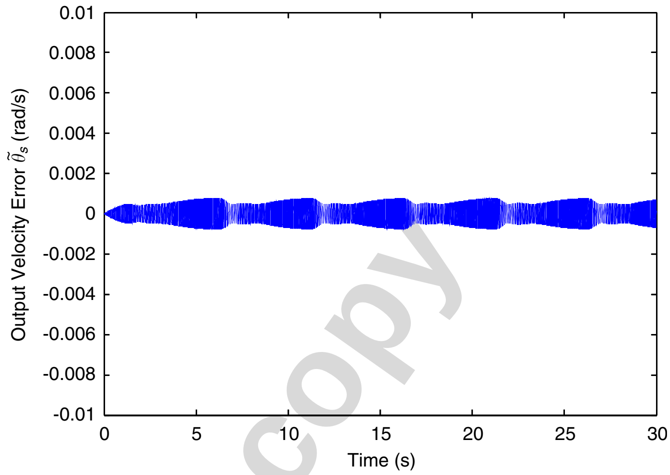

Fig. 13. Output velocity estimation error.

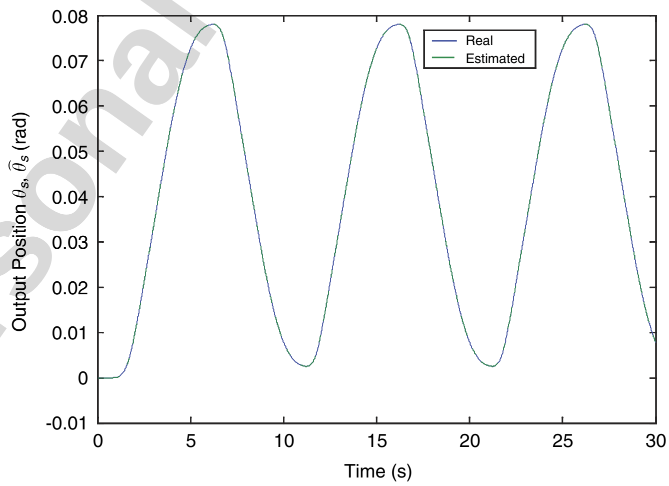

Fig. 14. Estimation of output position signal.

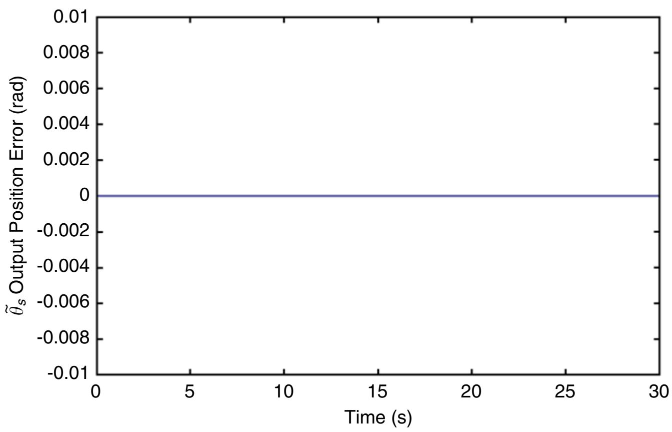

Fig. 15. Output position estimation error.

estimation of the output system part is illustrated in Figs. 12 and 14. These latter show the convergence of velocity and position errors asymptotically to zero (see Figs. 13 and 15). So, using the super-twisting algorithm, the dead zone magnitude and backlash transmitted torque have been identified and estimated respectively (see Fig. 16). Also, due to reconstruction of the system states

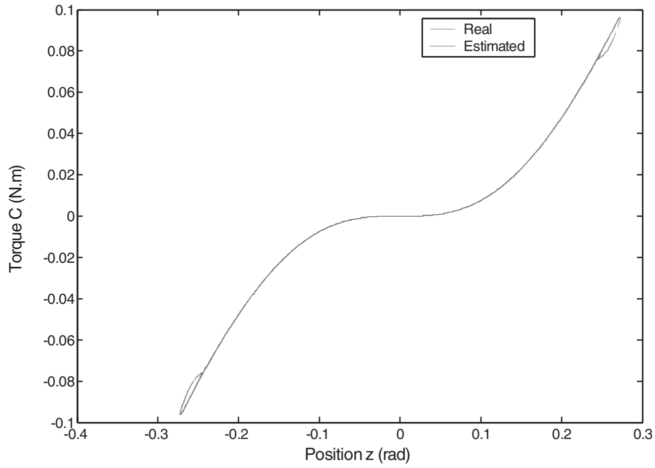

Fig. 16. Dead zone estimation.

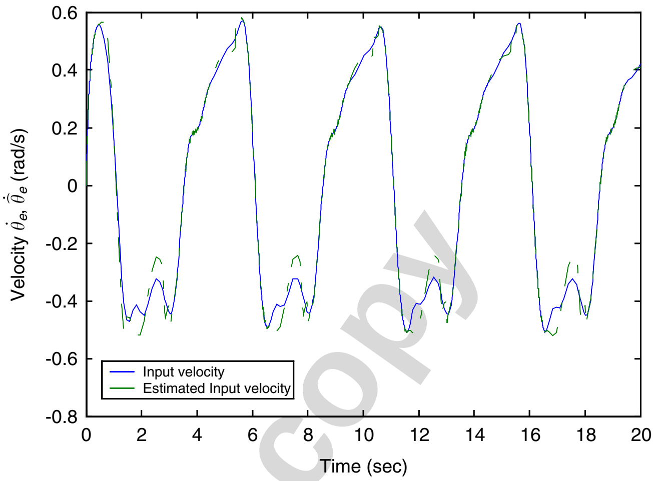

Fig. 18. Estimation of input velocity signal.

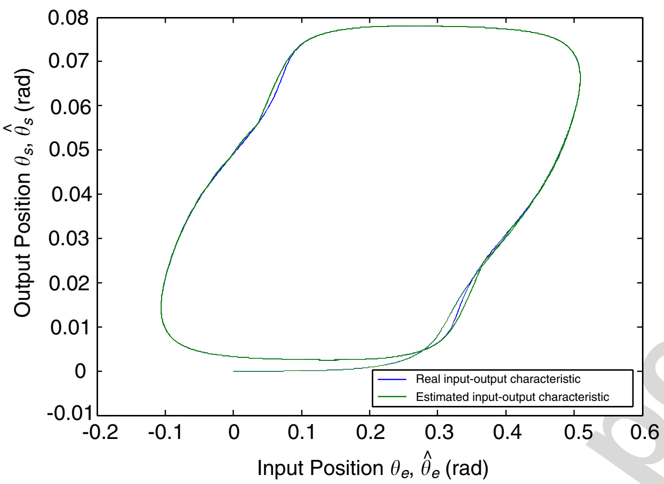

Fig. 17. Backlash input–output characteristic.

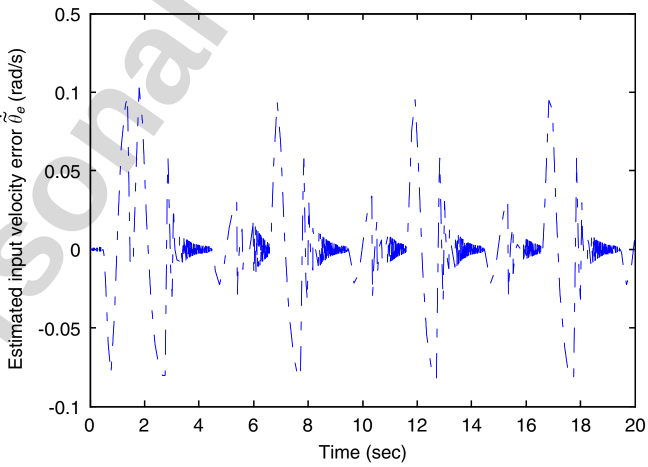

Fig. 19. Input velocity estimation error.

Table 2
Experimentation parameters

Observers parameters	
α_1	0.15
α_2	0.025
λ_1	0.01
λ_2	0.004

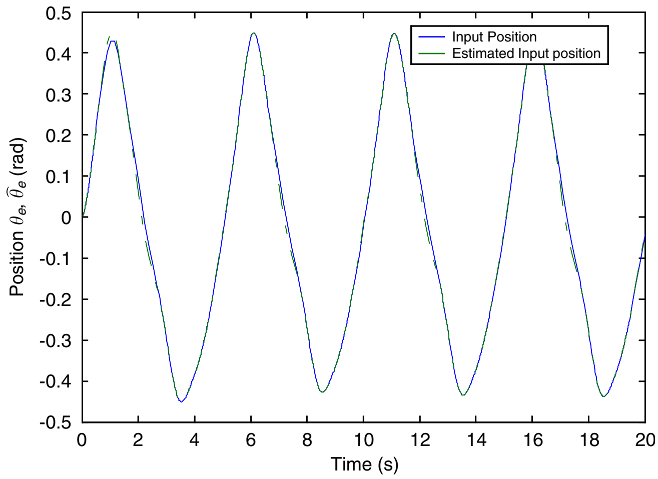

Fig. 20. Estimation of input position signal.

via the considered observers, the disturbing position hysteresis has been well identified as shown in Fig. 17.

6. Experimental results

Experimental tests have been done on the electromechanical test bench (see Fig. 1) described in Section 2, with the observer parameters given in Table 2. Only two states are measured, corresponding to positions of the motor axes (input position) and reducer part (output position). The proposed observers reconstruct input and output velocities of backlash phenomenon from the already performed input and output position measurements. Fig. 18 shows the real input velocity signal (continuous line) and its estimation through the corresponding observer (dotted line), where the estimation error converges to zero with less variations

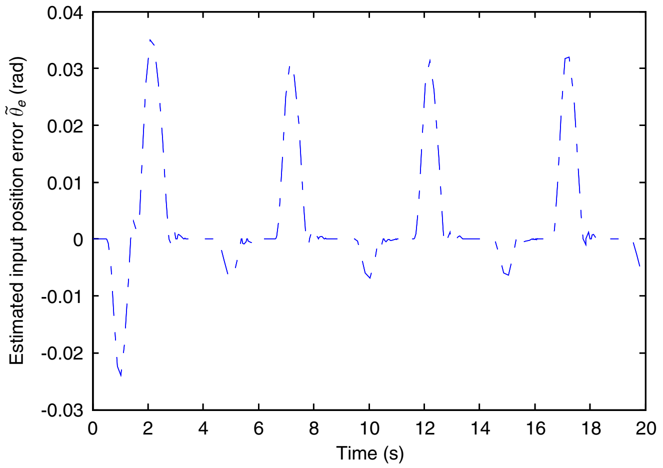

Fig. 21. Input position estimation error.

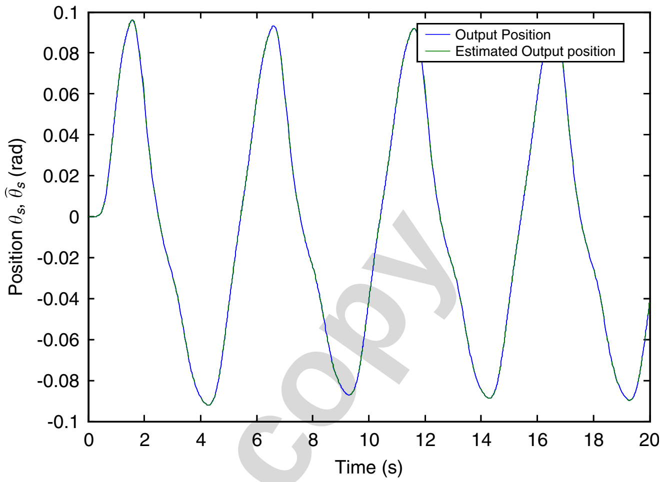

Fig. 24. Estimation of output position signal.

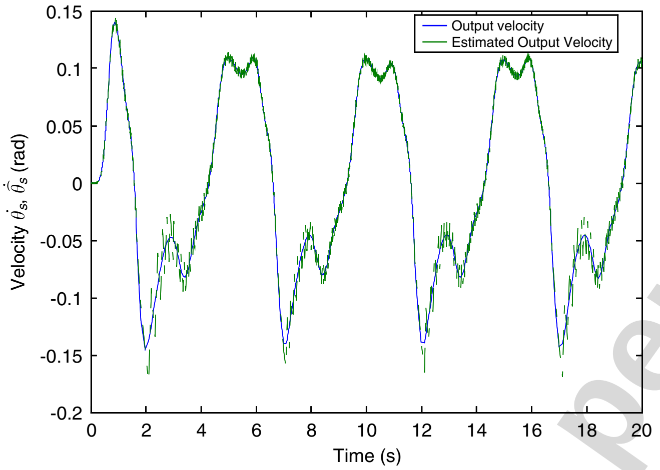

Fig. 22. Estimation of output velocity signal.

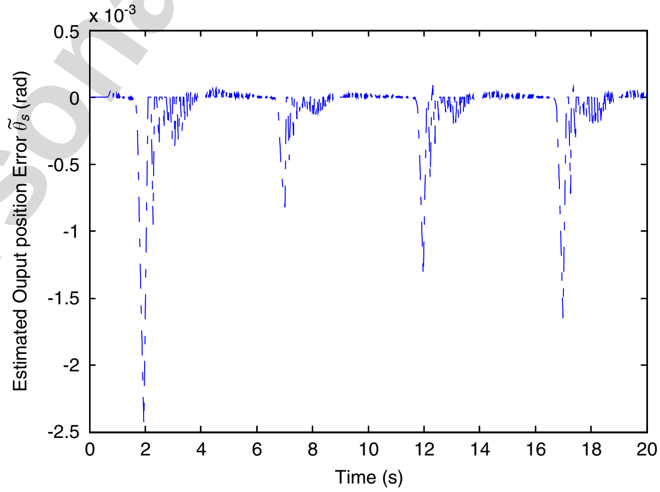

Fig. 25. Output position estimation error.

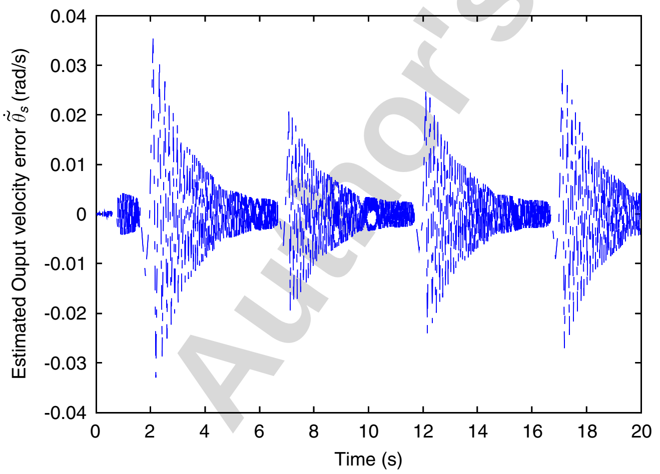

Fig. 23. Output velocity estimation error.

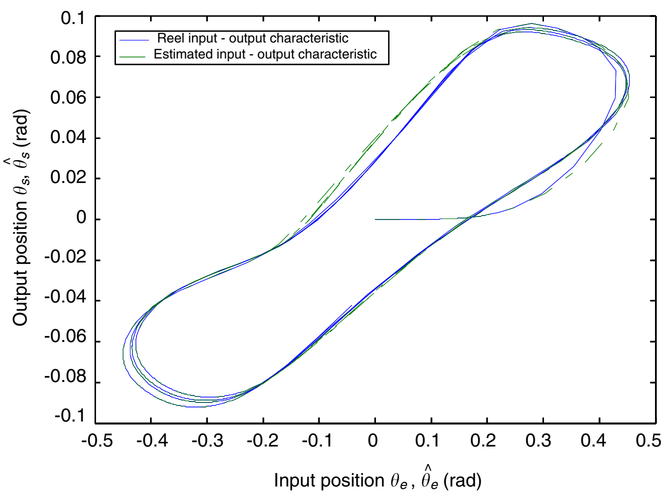

Fig. 26. Backlash input–output characteristic.

(see Fig. 19). Then, input position is deduced from the velocity estimation. It approaches to the real one, see Fig. 20, after convergence insurance of estimation error presented in Fig. 21. In a similar way as the input velocity, the output velocity (see Fig. 22) is estimated via its corresponding observer with a finite time convergence as shown in Fig. 23. Convergence of position error is described in Figs. 24 and 25 (see also Fig. 26). The robustness of the proposed observers is illustrated in Fig. 27, by a good reconstruction of the dead zone phenomenon. Ultimately, Fig. 28 shows the limit cycles of the backlash system after reconstruction.

7. Conclusion

In this work, a second order sliding mode observer ensuring the finite time convergence of estimated state values towards real state values is implemented in a nonlinear mechanical system with backlash phenomenon. The experimental results show the good performance of these observers in a real frame. The knowledge of equivalent control allows to identify the backlash phenomenon as perturbation. In a nonperturbed environment, the equivalent control permits the direct usage of the linear regression algorithms for the backlash parameters identification. Simulation and experimental tests support the theoretical development.

Appendix A. Convergence proof

Each couple of system (2) coordinates (x_{1e}, x_{2e}) and (x_{1s}, x_{2s}) has the following representation:

$$\begin{cases} \dot{x}_1 = x_2, \\ \dot{x}_2 = f(t, x_1, x_2, u) + \xi(t, x_1, x_2), \\ y = x_1. \end{cases} \tag{29}$$

For the system under the form (29), the super-twisting observer is expressed as

$$\begin{cases} \dot{\hat{x}}_1 = \hat{x}_2 + z_1, \\ \dot{\hat{x}}_2 = f(t, x_1, \hat{x}_2, u) + z_2, \end{cases} \tag{30}$$

where $\hat{x}_1$ and $\hat{x}_2$ are the state estimations, z_1 and z_2 are the correction factors based on the super-twisting algorithm and are given by the formulas

$$\begin{cases} z_1 = \lambda |x_1 - \hat{x}_1|^{1/2} \operatorname{sign}(x_1 - \hat{x}_1), \\ z_2 = \alpha \operatorname{sign}(x_1 - \hat{x}_1). \end{cases} \tag{31}$$

Assume that

$$|f(t, x_1, x_2, u) - f(t, x_1, \hat{x}_2, u) + \xi(t, x_1, x_2)| \leqslant f^+.$$

Then α and λ satisfy the inequalities

$$\begin{cases} \alpha > f^+, \\ \lambda > \sqrt{\dfrac{2}{\alpha - f^+}} \dfrac{(\alpha + f^+)(1+q)}{(1-q)}, \end{cases} \tag{32}$$

where q is some chosen constant in the interval $0 < q < 1$.

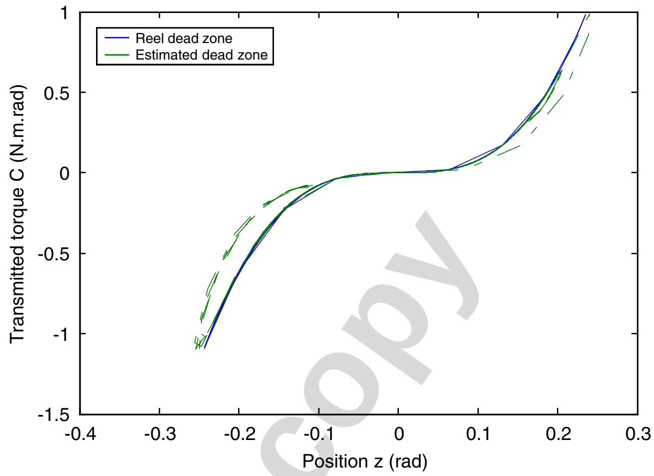

Fig. 27. Dead zone estimation.

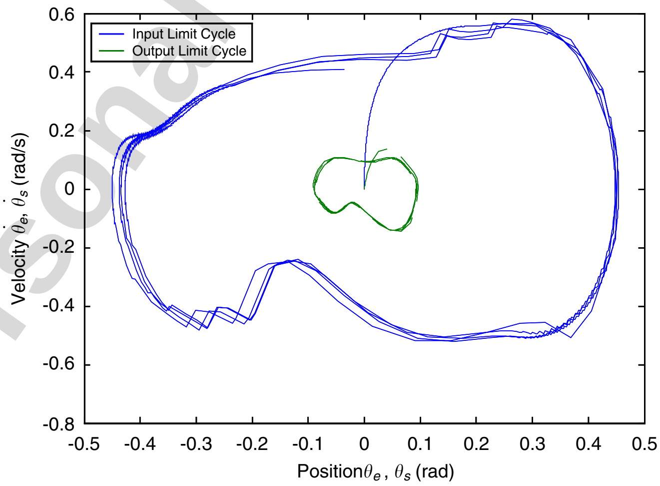

Fig. 28. Backlash limit cycle estimation.

To prove the convergence of the state estimates to the real states, it is first necessary to prove the convergence of $\tilde{x}_1$ and $\dot{\tilde{x}}_1$ to zero. Computing the derivative of $\dot{\tilde{x}}_1$, then the following is obtained:

$$\ddot{\tilde{x}}_1 = g(t, x_1, x_2, \hat{x}_2, u) - \frac{\lambda}{2} \dot{\tilde{x}}_1 |\tilde{x}_1|^{-1/2} - \alpha \operatorname{sign}(\tilde{x}_1). \tag{33}$$

The trivial identity $(\mathrm{d}/\mathrm{d}t)|x| = \dot{x} \operatorname{sign} x$ is used here. The latter equation may be rewritten as

$$\ddot{\tilde{x}}_1 \in [-f^+, f^+] - \left(\frac{1}{2} \lambda \frac{\dot{\tilde{x}}_1}{|\tilde{x}_1|^{1/2}} + \alpha \operatorname{sign} \tilde{x}_1 \right). \tag{34}$$

The inclusion (34) does not "remember" anything of the real system, but can be used to describe the majorant curve drawn in Fig. 29. In case when $\tilde{x}_1 > 0$ and $\dot{\tilde{x}}_1 > 0$, the trajectory is confined between the axis $\tilde{x}_1 = 0$, $\dot{\tilde{x}}_1 = 0$ and the trajectory of the equation $\ddot{\tilde{x}}_1 = -(\alpha - f^+)$. Let $\tilde{x}_{1_M}$ be the intersection of this curve with the axis $\dot{\tilde{x}}_1 = 0$. Obviously, $2(\alpha - f^+)\tilde{x}_{1_M} = \dot{\tilde{x}}_{1_0}^2$. It is easy to see that for

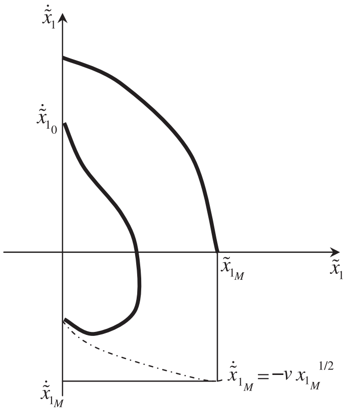

Fig. 29. Majorant curve for finite time convergence observer.

$\tilde{x}_1 > 0, \dot{\tilde{x}}_1 > 0$

$$\ddot{\tilde{x}}_1 \leqslant f^+ - \alpha\,\text{sign}(\tilde{x}_1) - \frac{1}{2}\lambda\,\frac{\dot{\tilde{x}}_1}{|\tilde{x}_1|^{1/2}} < 0. \tag{35}$$

Thus the trajectory approaches the axis $\dot{\tilde{x}}_1 = 0$.

The majorant curve for $\tilde{x}_1 > 0, \dot{\tilde{x}}_1 \geqslant 0$ is described by the equation (see Fig. 29)

$$\dot{\tilde{x}}_1^2 = 2(\alpha - f^+)(\tilde{x}_{1_M} - \tilde{x}_1) \quad \text{for } \dot{\tilde{x}}_1 > 0. \tag{36}$$

The majorant curve for $\tilde{x}_1 > 0, \dot{\tilde{x}}_1 \leqslant 0$ consists of two parts. In the first part the point instantly drops down from $(\tilde{x}_{1_M}, 0)$ to the point $(\tilde{x}_{1_M}, -(2/\lambda)(f^+ + \alpha)\tilde{x}_{1_M}^{1/2}$, where the right hand side of inclusion (34) in the 'worst case' is equal to zero. The second part of majorant curve is the horizontal segment between the points $(\tilde{x}_{1_M}, -(2/\lambda)(f^+ + \alpha)\tilde{x}_{1_M}^{1/2}) = (\tilde{x}_{1_M}, \dot{\tilde{x}}_{1_M})$ and $(0, \dot{\tilde{x}}_{1_M})$.

Condition (32) implies that

$$\frac{|\dot{\tilde{x}}_{1_M}|}{|\dot{\tilde{x}}_{1_0}|} < \frac{1-q}{1+q} < 1. \tag{37}$$

Inequality (37) ensures the convergence of the state $(\tilde{x}_{1_i}, \dot{\tilde{x}}_{1_i})$ to $\tilde{x}_1 = \dot{\tilde{x}}_1 = 0$ and, moreover, the convergence of $\sum_0^\infty |\dot{\tilde{x}}_{1_i}|$. To prove the convergence finite time, consider the dynamics of $\tilde{x}_2$. Obviously, $\tilde{x}_2 = \dot{\tilde{x}}_1$ at the moments when $\tilde{x}_1 = 0$ and taking into account that

$$\dot{\tilde{x}}_2 = g(x_1, x_2, \hat{x}_2, u) - \alpha\,\text{sign}(\tilde{x}_1) \tag{38}$$

obtain

$$0 < \alpha - f^+ \leqslant |\dot{\tilde{x}}_2| \leqslant \alpha + f^+ \tag{39}$$

holds in a small vicinity of the origin. Thus

$$|\dot{\tilde{x}}_{1_i}| \geqslant (\alpha - f^+)t_i, \tag{40}$$

where t_i is the time interval between the successive intersection of the trajectory with the axis $\tilde{x}_1 = 0$. Hence

$$t_i \leqslant \frac{|\dot{\tilde{x}}_{1_i}|}{(\alpha - f^+)} \tag{41}$$

and the total convergence time is given by

$$T \leqslant \sum \frac{|\dot{\tilde{x}}_{1_i}|}{(\alpha - f^+)}. \tag{42}$$

So T is finite and the estimated states converge to the real states in finite time.

References

Allan, P., & Levy, N. (1980). The Determination of pre-load for antibacklash gears in a positional servomechanism. *IEEE Transactions on Industrial Electronics*, *27*, 26–29.

Almeida, D., & Alvarez, J. (2004). Robust synchronization of a class of nonlinear systems. *Proceedings of 2004 American control conference* (pp. 1259–1265). Boston, USA, June 30–July 2, 2004.

Barbosa, R. S., & Tenreiro Machado, J. A. (2002). Describing function analysis of systems with impacts and backlash. *Nonlinear Dynamics*, *29*, 235–250.

Davila, J., & Fridman, F. (2004). Observation and identification of mechanical systems via second order sliding modes. *Proceedings of the eighth international workshop on variable structure systems* (*VSS '04*), September 6–8, 2004, Vilanova i la Geltru, Spain.

Dixon, R. (2004). Observer-based FDIA: Application to an electromechanical positioning system. *Control Engineering Practice*, *12*(9), 1113–1125.

Lambrechts, P., Boerlage, M., & Steinbuch, M. (2005). Trajectory planning and feedforward design for electromechanical motion systems. *Control Engineering Practice*, *13*(2), 145–157.

Levant, A. (1993). Sliding order and sliding accuracy in sliding mode control. *International Journal of Control*, *58*, 1247–1263.

Levant, A. (1998). Robust exact differentiation via sliding mode technique. *Automatica*, *34*, 379–384.

Merzouki, R., & Cadiou, J. C. (2005). Estimation of backlash phenomenon in the electromechanical actuator. *Journal of Control Engineering Practice*, *13*(8), 973–983.

Merzouki, R., Cadiou, J. C., & M'Sirdi, N. K. (2004). Compensation of friction and backlash effects in an electrical actuator. *Journal of Systems and Control Engineering*, *218*(12), 75–84.

Orlov, Y., Alvarez, J., & Acho, A. (2000). An invariance principle for discontinuous dynamic systems with application to a coulomb friction oscillator. *Journal of Dynamic Systems, Measurement and Control*, *122*, 687–690.

Shaw, J., & Rand, S. R. H. (1989). The transition to chaos in a simple mechanical system. *Journal of Nonlinear Mechanics*, *24*, 41–56.

Shtessel, S., Shkolnikov, I. A., & Brown, M. D. J. (2003). An asymptotic second-order smooth sliding mode control. *Asian Journal of Control*, *5*, 498–504.

Soderstrom, T., & Stoica, P. (1989). *System identification*. Englewood Cliffs, NJ: Prentice-Hall International.

Tao, G., & Kokotovic, P. V. (1995). Continuous-time adaptive control of systems with unknown backlash. *IEEE Transactions on Automatic Control*, *40*, 1083–1087.

Tenreiro Machado, J. A. (1996). Variable structure control of manipulators with joints having flexibility and backlash. *Journal Systems Analysis-Modelling-Simulation*, *23*, 93–101.

Thompson, J. M. T., & Ghaffari, R. (1982). Chaos after period-doubling bifurcations in the resonance of an impact oscillator. *Physical Letters*, *91*.

Utkin, V., Guldner, J., & Shi, J. (1999). *Sliding mode control in electromechanical systems*. London, UK: Taylor & Francis.